Iterative Narrowband-Based Graph Cuts Optimization for Geodesic Active Contours With Region Forces (GACWRF)

Wenbing Tao

***Abstract*—In this paper, an iterative narrow-band-based graph cuts (INBBGC) method is proposed to optimize the geodesic active contours with region forces (GACWRF) model for interactive object segmentation. Based on cut metric on graphs proposed by Boykov and Kolmogorov, an NBBGC method is devised to compute the local minimization of GAC. An extension to an iterative manner, namely, INBBGC, is developed for less sensitivity to the initial curve. The INBBGC method is similar to graph-cuts-based active contour (GCBAC) presented by Xu *et al.*, and their differences have been analyzed and discussed. We then integrate the region force into GAC. An improved INBBGC (IINBBGC) method is proposed to optimize the GACWRF model, thus can effectively deal with the concave region and complicated real-world images segmentation. Two region force models such as mean and probability models are studied. Therefore, the GCBAC method can be regarded as the special case of our proposed IINBBGC method without region force. Our proposed algorithm has been also analyzed to be similar to the Grabcut method when the Gaussian mixture model region force is adopted, and the band region is extended to the whole image. Thus, our proposed IINBBGC method can be regarded as narrow-band-based Grabcut method or GCBAC with region force method. We apply our proposed IINBBGC algorithm on synthetic and real-world images to emphasize its performance, compared with other segmentation methods, such as GCBAC and Grabcut methods.**

***Index Terms*—Geodesic active contours (GAC), graph cuts, iterative algorithm, narrowband, region forces.**

I. Introduction

IMAGE segmentation is an important problem in computer vision, which involves the extraction of an interest region from an image and segment the image into foreground and background. The interest region may include one object or multiple objects, which is useful for a further image analysis task such as medical application and scene understanding. Various variational and partial differential equations (PDEs)-based methods have been proposed to extract interest objects in images such as the well-known and successful active contour/snake model, initially proposed by Kass *et al.* [1]. The segmentation based on variational framework is extensively applied to interactive object extraction since accurately defining the desired object boundaries or regions completely automatically is a difficult task by using the current technologies. Here, we focus on object boundary detection by a dynamic model known as the geodesic active contour (GAC), which was proposed in [2] and [40] as a simplification of the snake energy model with fewer parameters and less sensitivity to the initial contour.

This GAC segmentation technique is based on geodesics in a Riemannian space with a metric induced by the image content. Then, simple closed curves with minimal energy are used to segment a specific object from the image. A variational framework based on steepest descent of energy functional is used to obtain locally minimal contours. Caselles *et al.* [2] used a direct first-order time scheme for the level set PDE, and the timestep in this scheme was dictated by stability requirements. Goldenberg *et al.* [3] adapted the additive operator splitting scheme [5] to obtain an unconditionally stable update for the narrow-band level set method, greatly increasing the speed of the segmentation. However, variational descent methods are prone to becoming stuck in local minimum caused by noise or local disturbance such as the shadow in the image, the change of the illumination in the background, or the heterogeneity of the object. Although some strategies have been proposed to avoid the local minima and offer improved robustness [4], [6], [40], the sensitivity to initialization is still not solved.

To overcome the local characteristic of the GAC, Cohen and Kimmel [7] formulate the GAC as a search for minimal geodesics in Riemannian space, and the fast marching algorithm [8] is applied to obtain minimal paths. However, their formulation only locates the boundary of an object as the open geodesic connecting two user-specified points. This paper is further extended to detect open and closed contours connecting a number of seed points in an image [9]. Similarly, Appleton and Talbot [10] use the fast marching algorithm combined with a branch and bound search for connected endpoints to obtain the minimum closed geodesic containing a specified internal point. However, the need of a specified internal point can limit the segmentation process because it means that object with multiple closed curves cannot be extracted without a set of seed points. Bresson *et al.* [11] propose to unify three well-known image variational models, namely, the snake model

Manuscript received April 25, 2010; revised March 09, 2011; accepted June 07, 2011. Date of publication June 30, 2011; date of current version December 16, 2011. This work was supported in part by the National Natural Science Foundation of China under Grant 61073093 and in part by the Fundamental Research Funds for the Central Universities of China through Huazhong University of Science and Technology under Grant 2010MS025. The associate editor coordinating the review of this manuscript and approving it for publication was Prof. Sabine Susstrunk.

The author is with the Institute for Pattern Recognition and Artificial Intelligence and State Key Laboratory for Multi-spectral Information Processing Technologies, Huazhong University of Science and Technology, Wuhan 430074, China.

Color versions of one or more of the figures in this paper are available online at http://ieeexplore.ieee.org.

Digital Object Identifier 10.1109/TIP.2011.2160955

[1], [2], the Rudin–Osher–Fatemi denoising model [12], and the Mumford–Shah segmentation model [13], [14] and prove the existence of a global minimum of the active contour model. Then, a practical way to solve the active contour propagation problem toward object boundaries through a dual formulation of the minimization problem is proposed.

We study image segmentation based on variational framework such as active contour model [1], [2] and their graph cuts optimization in this paper. The graph cuts method was first introduced into computer vision as an optimizing tool by Greig *et al.* [15] in connection with Markov random fields (MRFs). It has later been studied by [16]–[18]. By optimizing the energy function based on the maximization of the posterior probability and MRFs, some interactive image segmentation methods based on graph cuts [19], [20], [21], [34] have been proposed. Recently, the graph cuts method has also received a lot of attention due to its connection with continuous variational problem and PDEs [18], [22]–[25], [39]. In particular, El-Zehiry *et al.* [39] has applied graph cuts to optimize the CV model by Chan and Vese [36]. The basic idea of graph cut method is to construct a weighted graph structure $\mathbf{G} = (\mathbf{V}, \mathbf{E}, \mathbf{W})$, where $\mathbf{V}$ is the set of vertices, $\mathbf{E}$ is the set of edges, and $\mathbf{W}$ is the set of nonnegative weights on the edges. Then, solve the minimal cut problem and find a cut whose capacity is the minimum over all cuts of graph $\mathbf{G}$. If graph $\mathbf{G}$ is a flow network, i.e., a special directed graph with a source node and sink node, due to the max-flow min-cut theorem by Ford and Fulkerson [26], there are several fast algorithms to solve the minimal cut problem of graph $\mathbf{G}$ by solving the corresponding maximal flow problem such as the augmenting path style method [17], [27] or the push-relabel style method [28]. See [17] for a detailed discussion about the implementation and comparison of several algorithms.

In this paper, we first deduce the discrete representation of the GAC based on cut metric theory on graphs [22], [38] and analyze the equivalence between the minimization of the GAC and the minimum cut problem. We notice that the global minimum of the GAC model corresponds to a point, which has no practical sense for the image segmentation task [11]. This is consistent with the minimum cut that favors cutting the isolated nodes [29], [30]. To obtain meaningful local minimization of the GAC, we develop a narrow-band-based on graph cuts (NBBGC) method to solve the local minimization of the GAC for higher efficiency and better accuracy than the traditional level set framework [32], [33]. The NBBGC method can be easily extended to an iterative manner, i.e., iterative NBBGC (INBBGC), for less sensitivity to the initial curve placed by user. Although the INBBGC method is somewhat similar to the graph-cuts-based active contours (GCBAC) method [31], INBBGC algorithm has a good theoretical basis and is the natural conclusion deduced by solving the minimizing problem of the GAC using graph cuts framework. However, in [31], the GCBAC algorithm is just constructed, but the inherent relationship between this algorithm and the GAC is not mentioned and clarified.

Due to the intrinsic limitation of energy function defined by the GAC, whose minimization is decided by the length and gradient of the evolving curve, the GAC has bias to segment the smaller region or isolated point set, which is consistent with minimum cut principle [29], [30]. Therefore, although the INBBGC algorithm has good performance when dealing with some simple images, lack of the region information makes the method fail to deal with the images with narrow and deep concave regions and the complicated natural scene images. To overcome this problem, we integrate region information into the GAC and develop an improved INBBGC (IINBBGC) algorithm to optimize the GACs with region forces (GACWRF) model. The IINBBGC algorithm includes not only the boundary forces derived from the GAC but also the region forces derived from the region features inside and outside the evolving curve and, thus, can effectively deal with the narrow and deep concave regions in an image. Two region force models, such as mean model (MM) and probability model (PM) are studied. Our proposed IINBBGC algorithm has been also analyzed to be similar to the Grabcut method when Gaussian mixture model (GMM) region force is adopted, and the band region is extended to the whole image. Therefore, our proposed IINBBGC algorithm can be regarded as a narrow-band-based Grabcut method or GCBAC with region force method. We apply our proposed algorithm on synthetic and real-world images to emphasize its performance, compared with other segmentation methods, such as the GCBAC and Grabcuts methods.

The outline of this paper is as follows: In the next section, we use cut metric theory to deduce the discrete representation of the GAC and show the equivalence between the minimization of the GAC and the minimum cut. In Section III, we develop an NBBGC to effectively solve the local minimization of the GAC. Then, an extended iterative version, i.e., the INBBGC, is proposed for less sensitivity to the initial curve. In Section IV, we integrate region information into the GAC and develop an IINBBGC algorithm to optimize the GACWRF model, and two region force models are developed. In Section V, we validate our proposed IINBBGC algorithm by various numerical results on synthetic images and real natural images, showing the advantages of our proposed algorithm, followed by a brief conclusion section in Section VI.

II. Graph Cuts Formulation for the GAC

Given the image domain $\Omega \subset \Re^2$, let $u_0 : \Omega \to \Re$ be a given image. Let C be a closed subset in Ω, made up of a finite set of smooth curves. We denote the length of curves making up C by $L(C)$. Let the set inside curve C be Ω_1 and the set outside C be Ω_2. The GAC is defined along curve C and minimized by evolving the curve in the normal direction, i.e.,

$$E_b(C) = \int_0^{L(C)} g\left(C(s)\right) ds. \tag{1}$$

The function g is an edge indicator function that vanishes at object, defined as follows:

$$g(u_0) = \frac{1}{1 + \beta \left|\nabla u_0\right|} \tag{2}$$

where β is an arbitrary positive constant and u_0 is the observed original image.

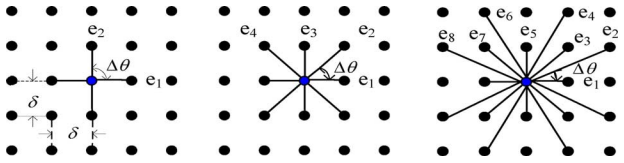

Fig. 1. (Left) 4 n-system. (Middle) 8 n-system. (Right) 16 n-system.

Therefore, energy functional (1) is actually a new length obtained by weighting the Euclidean element of length ds by functional g, which contains information concerning the boundaries of object [2].

Given a graph, i.e., $\mathbf{G} = (\mathbf{V}, \mathbf{E}, \mathbf{W})$, where $\mathbf{V}$ is the set of vertices, $\mathbf{E}$ is the set of edges, and $\mathbf{W}$ is the set of nonnegative weights on the edges. A cut on $\mathbf{G}$ is a partition of vertices $\mathbf{V}$ into two disjoint sets $\mathbf{S}$ and $\mathbf{T}$. For a given cut $(\mathbf{S}, \mathbf{T})$, the cost of the cut is defined as

$$|C|_G = \sum_{p \in S, q \in T} \omega_{pq} \tag{3}$$

where ω_{pq} is the weight of edge connecting nodes p and q.

Consider a cut on grid-graph $\mathbf{G}$ as a closed contours (in R^2). Length can be defined as the cut of $\mathbf{G}$ by (3), which is named as cut metric on graphs [22], [38]. By a Cauchy–Crofton formula, the connection between Euclidean length $|C|_E$ of curve C in R^2 and a measure of a set of lines intersecting it can be established. $\int n_L dL = 2|C|_E$, where $|C|_E$ is the Euclidean length and n_L is the number of times that line L intersects contour C. A neighborhood system of regular grid G in Fig. 1 can be described by a set $N_G = \{e_k : 1 \le k \le n_G\}$, where e_k is the direction vector and n_G is the number of the directions in the neighborhood system. Let $\Delta\phi$ be the angular differences between the nearest families of edge lines. In Fig. 1, $n_G = 2$ and $\Delta\phi = \pi/2$ for 4 n-system, $n_G = 4$ and $\Delta\phi = \pi/4$ for 8 n-system, and $n_G = 8$ and $\Delta\phi = \pi/8$ for 16 n-system. By some reasonably partitioning, the following discrete formula can be used to approximate the length of the contours:

$$|C|_E = \sum_{k=1}^{n_G} n_c(k) \cdot \frac{\delta^2 \cdot \Delta\phi_k}{2 \cdot |e_k|} \tag{4}$$

where $n_c(k)$ is the total number of intersections of C with the edge lines in the kth direction vector, i.e., e_k. Then, $\sum_{k=1}^{n_G} n_c(k)$ is the total number of the intersections of C with the edge lines. If we choose constant edge weights within each family of edge lines as

$$\omega_k = \frac{\delta^2 \cdot \Delta\phi_k}{2 \cdot |e_k|} \tag{5}$$

therefore, we have

$$|C|_E = \sum_{k=1}^{n_G} n_c(k) \cdot \omega_k \approx |C|_G. \tag{6}$$

We now use cut metric to discretize formula (1) to take values on a uniform grid so that they can be applied in image domain Ω. Let $P = \{(i,j) | i \in \{1, \ldots, n\}, j \in \{1, \ldots, m\}\}$ be the set of image grid points and $\delta = 1$ be the mesh size, $N = mn$ is the number of the grid points in P. Let each image pixel be a vertex, and the neighboring vertices are connected by edges with nonnegative weights. Then, image u_0 corresponds to graph $\mathbf{G} = (\mathbf{V}, \mathbf{E}, \mathbf{W})$, where $\mathbf{V}$ is the set of vertices, $\mathbf{E}$ is the set of edges, and $\mathbf{W}$ is the set of nonnegative weights on the edges. Consider all the pixels $\{u_0(i,j), (i,j) \in \Omega\}$ and define one binary variable x_{ij} in the image grid as follows:

$$x_{ij} = \begin{cases} 1, & (i,j) \in \Omega_1 \\ 0 & (i,j) \in \Omega_2 \end{cases}. \tag{7}$$

For simpler expression, let $p = (i,j) \in \Omega$; then, we have

$$ds = \omega_{pq} = \omega_k \tag{8}$$

where $x_p \neq x_q$ and $p \in N(q)$, $(p,q) \in e_k$, and $k = 1, \ldots, n_G$.

Therefore, the discrete form of the length of curve $L(C) = \int_0^{L(C)} ds$ can be expressed using cut metrics as follows:

$$L'(C) = |C|_G = \sum_{p,q \in \Omega} \sum_{p \in N(q)} \omega_{pq} \left((1 - x_p)x_q + x_p(1 - x_q)\right). \tag{9}$$

Define the gradient of $u_0(i,j)$ in a four n-system (shown in Fig. 1-left) and an eight n-system (shown in Fig. 1-middle) as

$$\begin{aligned} \nabla u_0(i,j) = {} & |u_0(i+1,j) - u_0(i,j)| \frac{e_1}{|e_1|} \\ & + |u_0(i,j+1) - u_0(i,j)| \frac{e_2}{|e_2|} \end{aligned} \tag{10}$$

$$\begin{aligned} \nabla u_0(i,j) = {} & |u_0(i+1,j) - u_0(i,j)| \frac{e_1}{|e_1|} \\ & + |u_0(i+1,j+1) - u_0(i,j)| \frac{e_2}{|e_2|} \\ & + |u_0(i,j+1) - u_0(i,j)| \frac{e_3}{|e_3|} \\ & + |u_0(i-1,j+1) - u_0(i,j)| \frac{e_4}{|e_4|} \end{aligned} \tag{11}$$

where $e_i/|e_i|, i = 1, \ldots, 4$ is the direction vector shown in Fig. 1.

Therefore, ∇u_0 in a four n-system and an eight n-system are respectively as follows:

$$\begin{aligned} \nabla u_0 = \sum_{i,j \in \Omega} \Big\{ & |u_0(i+1,j) - u_0(i,j)| \frac{e_1}{|e_1|} \\ & + |u_0(i,j+1) - u_0(i,j)| \frac{e_2}{|e_2|} \Big\} \end{aligned} \tag{12}$$

$$\begin{aligned} \nabla u_0 = \sum_{i,j \in \Omega} \Big\{ & |u_0(i+1,j) - u_0(i,j)| \frac{e_1}{|e_1|} \\ & + |u_0(i+1,j+1) - u_0(i,j)| \frac{e_2}{|e_2|} \\ & + |u_0(i,j+1) - u_0(i,j)| \frac{e_3}{|e_3|} \\ & + |u_0(i-1,j+1) - u_0(i,j)| \frac{e_4}{|e_4|} \Big\}. \end{aligned} \tag{13}$$

Notice that we ignore the boundary effect of the image grid in (10)–(13). Then, we have

$$g(u_0) = \frac{1}{1+\beta|\nabla u_0|} = \sum_{i,j\in\Omega}\left\{\frac{1}{1+\beta\,|u_0(i+1,j)-u_0(i,j)|} + \frac{1}{1+\beta\,|u_0(i,j+1)-u_0(i,j)|}\right\} \quad (14)$$

$$g(u_0) = \sum_{i,j\in\Omega}\left\{\frac{1}{1+\beta\,|u_0(i+1,j)-u_0(i,j)|} + \frac{1}{1+\beta\,|u_0(i+1,j+1)-u_0(i,j)|} + \frac{1}{1+\beta\,|u_0(i,j+1)-u_0(i,j)|} + \frac{1}{1+\beta\,|u_0(i-1,j+1)-u_0(i,j)|}\right\}. \quad (15)$$

By $p=(i,j)\in\Omega$ and (7), therefore, we have

$$g\left(C(s)\right) = \sum_{p,q\in\Omega}\sum_{p\in N(q)}\frac{(1-x_p)x_q + x_p(1-x_q)}{1+\beta\,|u_0(p)-u_0(q)|}. \quad (16)$$

Combining (9) and (16), discrete representation $E_b'(C)$ of $E_b(C)$ in (1) can be obtained as follows:

$$E_b'(C) = \sum_{p,q\in\Omega}\sum_{p\in N(q)}\frac{\omega_{pq}}{1+\beta\,|u_0(p)-u_0(q)|}\times\left((1-x_p)x_q + x_p(1-x_q)\right). \quad (17)$$

Given neighboring vertices p and q, let the weight of the edge connecting vertices p and q be

$$w_{pq} = \frac{\omega_{pq}}{1+\beta\,|u_0(p)-u_0(q)|}. \quad (18)$$

Then, the discrete representation of the GAC in (17) is actually a cut of graph $\mathbf{G}$ with the weights of the edges defined in (18). If this cut partition $\mathbf{G}$ into set $\mathbf{S}$ and $\mathbf{T}$, then $S=\{p: x_p=1\}$ and $T=\{p: x_p=0\}$. Therefore, minimizing $E_b'(C)$ is equivalent to the minimizing the cut problem of graph $\mathbf{G}$. Wu and Leahy [29] proposed a clustering method based on the minimum cut criterion, which yields good segmentation results but favors cutting to small sets of isolated nodes in a graph. To prevent such unnatural bias of cutting into small sets of nodes, Shi and Malik [30] proposed a new measure of disassociation between two groups, which is termed normalized cuts. Since we have proven the equivalence between minimization of the GAC and the minimum cut, minimizing the GAC also has the bias of segmenting small sets of isolated pixels in an image. The global minimum of the GAC model corresponds to a point, which has no practical sense for the image segmentation task [11]. This is consistent with the minimum cut that favors cutting the isolated nodes. In the next section, we will show that a useful local minimum of the GAC can be effectively obtained to segment image by using particularly devised NBBGC algorithm.

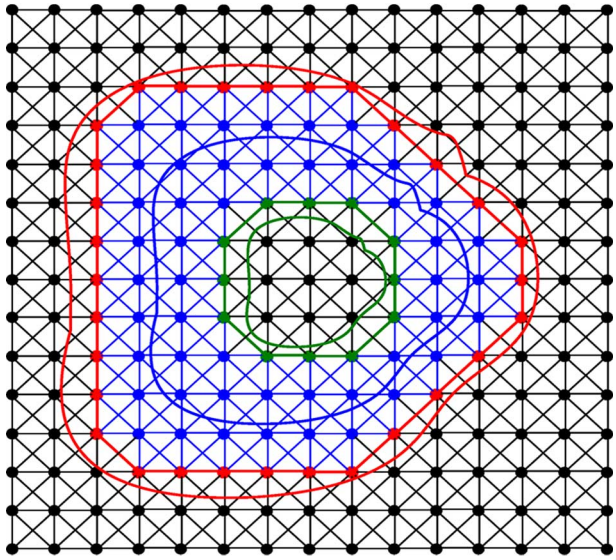

Fig. 2. (Blue curve) Initial curve placed by the user. The red nodes and edges, the green nodes and edges, and the blue nodes and edges compose band region R_b in the image after dilating the blue curve. The red nodes and edges and the green nodes and edges are, respectively, the exterior and interior boundaries of band region R_b.

III. Graph Cuts for Local Minimization of the GAC

Although minimizing the GAC can be transformed to an equivalent minimum cut problem, corresponding graph $\mathbf{G}$ must be a flow network in which the min-cut problem can be effectively solved. We will construct flow network graph $\mathbf{G}$ with one source node s and sink node t, and the GAC can be effectively minimized in $\mathbf{G}$.

A. NBBGC for Local Minimization of the GAC

Given initial curve C, which is the blue curve shown in Fig. 2, we dilate the curve to get a band region, i.e., named R_b, which is the region between the green curve and the red curve in Fig. 2, including the red nodes and edges, which compose the exterior boundary, the green nodes and edges, which compose the interior boundary, and the blue nodes and edges. We can construct graph $\mathbf{G}$ whose nodes correspond to the pixels in region R_b using the N_8 system shown in Fig. 2. The weights of the edges connecting these nodes with each other are set according to (18). We then design two special nodes, i.e., source node s and sink node t for $\mathbf{G}$. There are edges that connect the source node with the nodes in the exterior boundary, i.e., the red nodes shown in Fig. 2 and the edges that connect the sink node with the nodes in the interior boundary, i.e., the green nodes shown in Fig. 2, and the weights of these edges are infinite. Thus, graph $\mathbf{G}=(\mathbf{V},\mathbf{E})$ is a flow network (shown in Fig. 3), and vertices $\mathbf{V}$ can be partitioned into two disjoint sets, i.e., $\mathbf{S}$ and $\mathbf{T}$, such that $s\in S$ and

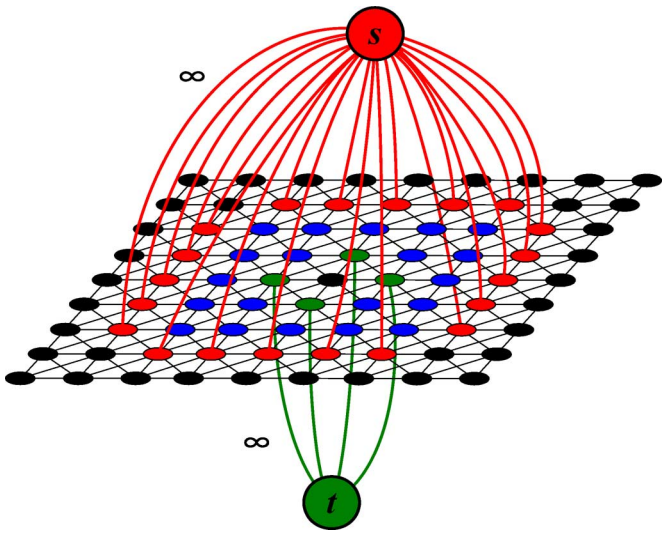

Fig. 3. Flow network graph $\mathbf{G}$ is constructed by band region R_b. The red nodes in the exterior boundary are connected with source node s, and the weights of these t-links are all infinite. The green nodes in the interior boundary are connected with sink node t, and the weights of these t-links are all infinite. The n-links are computed by (18).

$t \in T$ by some efficient min-cut algorithm [17], [27], [28]. Since the weights of the edges connecting the source node with the exterior boundary and connecting the sink node with the interior boundary are infinite, the interior boundary must belong to $\mathbf{T}$, and the exterior boundary must belong to $\mathbf{S}$. Therefore, the min-cut of band graph $\mathbf{G}$ corresponds to the minimization of the GAC in band region R_b of the image. This minimization is also one local minimum of the GAC in the whole image. Based on the min-cut, we can obtain close curve $C_{\min}$ that includes the interior boundary of band region R_b. This close curve $C_{\min}$ corresponds to the minimum cut of band graph $\mathbf{G}$ and partition the image into two parts, i.e., the interior of curve $C_{\min}$ and the exterior of curve $C_{\min}$.

We know that the wider band region R_b is, the closer to the global minimum in image the minimization of the GAC in R_b will be. Consider a special case where band R_b is extended to the whole image; in this case, the exterior boundary of flow network graph $\mathbf{G}$ corresponds to the boundary of the image, and the interior boundary of $\mathbf{G}$ degenerates to a node whose t-link with the sink node t has infinite weight. Thus, there is a high possibility that the minimum cut of this graph will only cut the isolated interior boundary node. This global minimum has no practical sense, as we previously said.

Due to the intrinsic limitations of the energy functional (17) derived from the GAC, it has a bias of converging to the interior boundary of band region R_b because less number of edges will be cut off in this case. Therefore, to avoid obtaining the meaningless local minimum, we must assume that the initial curve is as close to the expected object boundary as possible so as to make the formed band region R_b that includes the object boundary by dilating that the initial curve is as narrow as possible.

Based on the above discussion, we can construct the NBBGC algorithm as follows to segment image by minimizing the GAC.

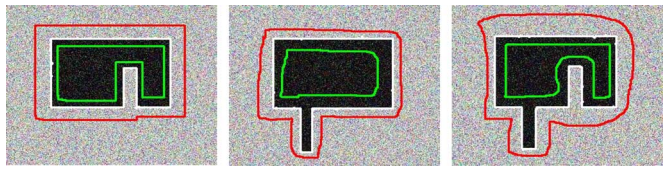

Fig. 4. Three types of images deal with by the NBBGC algorithm. (Left) Dilate 30 pixels toward outside to get band region R_b based on the initial green curve placed by the user. (Middle) Dilate 30 pixels toward inside to get band region R_b by the initial red curve. (Right) The interior green curve and exterior red curves are both placed by the users. (White curves) The local minimization of the GAC in band region R_b. The image size is 240 × 280.

NBBGC Algorithm:

1) Initialize curve C as near to the boundary of the interest object as possible;

2) Dilate curve C to form band region R_b, which includes the boundary to the interest object and is as narrow as possible.

3) Consider the pixels of band region R_b as the nodes of $\mathbf{G}$, and construct flow network graph $\mathbf{G}$ corresponding to R_b. The nodes in the interior boundary of $\mathbf{G}$ are connected with the sink node, and the nodes in the exterior boundary of $\mathbf{G}$ are connected with the source node. The weights of the n-links are computed according to (18), and the weights of the t-links are set infinite.

4) Compute minimum cut $(\mathbf{S}, \mathbf{T})$ with $s \in S = \{p : x_p = 1\}$ and $t \in T = \{p : x_p = 0\}$ of $\mathbf{G}$ using graph cuts algorithm, we can get close curve $C_{\min}$ corresponding to the minimization of the GAC.

5) Consider the pixels of the image region inside curve $C_{\min}$ as the foreground and the pixels of the image region outside curve $C_{\min}$ as the background. We can obtain the image segmentation results.

In practical applications, some simple extensions can be derived from the basic NBBGC, including the following three cases: 1) Given initial curve C, which is the blue curve shown in Fig. 2, we just dilate C toward the outside to get the band region R_b. In this case, see Fig. 2, the interior boundary of R_b is the initial blue curve, which is specified by the user, and the exterior boundary of R_b is the red curve. We place the initial curve inside the boundary of the interest object and is as near to it as possible. Thus, band region R_b is as narrow as possible and includes the boundary of the interest object. This case will be useful when the interest object includes the narrow and deep concave. Fig. 4(a) shows this case; 2) contrary to case 1, given initial curve C, we just dilate C toward the inside to get band region R_b. In this case, see Fig. 2, the interior boundary of R_b is the green curve, and the exterior boundary of R_b is the initial blue curve, which is specified by the user. This case will be useful when the interest object includes the thin and long structures. Fig. 4(b) shows this case; 3) a natural extension of cases 1 and 2 is that both the interior and exterior boundaries of band region R_b are specified by the user. This case will be useful when the interest object includes both the thin–long structures and the narrow–deep concave. Fig. 4(c) shows this case.

B. INBBGC for Minimization of the GAC

We have developed an NBBGC method to solve the local minimization of the GAC [2]. This method can easily be extended to an iterative manner so that the sensitivity to the initialized curve can be greatly decreased. We first describe the algorithm flow and then analyze some characteristics of the algorithm. Lastly, some related works will be discussed. The INBBGC can be summarized as follows.

INBBGC Algorithm:

1) Initialize curve C;

2) Dilate curve C to form a band region R_b;

3) Consider the pixels of band region R_b as the nodes of $\mathbf{G}$, and construct a flow network graph $\mathbf{G}$ corresponding to R_b. The nodes in the interior boundary of $\mathbf{G}$ are connected with the sink node, and the nodes in the exterior boundary of $\mathbf{G}$ are connected with the source node. The weights of the n-links are computed according to (18), and the weights of the t-links are set infinite;

4) Compute the minimum cut $(\mathbf{S}, \mathbf{T})$ with $s \in S = \{p : x_p = 1\}$ and $t \in T = \{p : x_p = 0\}$ of $\mathbf{G}$ using graph cuts algorithm, we can get close curve $C_{\min}$ corresponding to the minimization of the GAC;

5) Dilate curve $C_{\min}$ to update band region R_b;

6) Repeat from steps 3 to 5 until converges;

7) Consider the pixels of the image region inside curve $C_{\min}$ as the foreground and the pixels of the image region outside curve $C_{\min}$ as the background. We can obtain the image segmentation results.

The INBBGC algorithm is an iterative process between solving the minimum cut problem in band region R_b and updating R_b according to minimum cut curve $C_{\min}$. The minimization of the GAC is iteratively computed until it converges to the stable one. In all our experiment, this algorithm converged in 6–12 iterations. Notice that this stable solution is still a local minimization of the GAC in the whole image. In the iterative algorithm, width d of band region R_b needs to be decided by the user, which has an important effect on the result. The larger value of parameter d can obtain the smaller local minimization of the GAC because of larger search range. The experiment in Fig. 5 analyzes the relation between parameter d and the obtained local minimization of the GAC. From the experiments, we can see that due to the constraint of parameter d, the algorithm cannot jump out the current local minimum. A larger value of parameter d is helpful in obtaining smaller local minimum of the GAC. However, sometimes, the smaller local minimum of the GAC does not always correspond to the better segmentation, and as we have previously said, the GAC model has a bias to segment smaller region. Therefore, we should carefully select the value of parameter d and place the initial curve for the given application.

The INBBGC method proposed in this paper is somewhat similar to the GCBAC method in [31]. Both the two algorithms construct the graph based on the narrow-band region of the image and all the nodes in the graph have n-links connecting their neighbor nodes, but only the nodes in the exterior and interior boundaries have t-links. Then, the algorithms iteratively carry out between solving the minimum cut problem of the band graph and updating the band by dilating the minimum cut curve. In most object segmentation cases, the INBBGC method can obtain the same results as the GCBAC method [31] if the same initial curve is given for the two methods. However, the differences are three folds.

1) The motivations are absolutely different. Our INBBGC algorithm has a good theoretical basis and a natural conclusion that is deduced by solving the minimizing problem of the GAC using graph cuts framework. In [31], the GCBAC algorithm is just constructed, but the inherent relationship between this algorithm and the active contour is not mentioned and clarified.
2) The computation of the weights of the n-links is different. In the proposed INBBGC method, the computation of the weights of the n-link is strictly deduced from the cut metrics theory on graph [22] and the discrete representation of the GAC. In [31], the weights of the n-links are simply computed according to the image gradient.
3) The setup of the weights of t-links is different. In this proposed method, the weights of t-links are set infinite to assume that the interior boundary and the exterior boundary of the band graph are partitioned to different parts by the minimum cut of the band graph so that we can obtain a meaningful local minimization of the GAC, and the corresponding minimum cut curve includes the interior boundary curve. In [31], the constructed graph is actually an equivalence of a multiple-source and multiple-sink graph, where the multiple sources and the multiple sinks are, respectively, the neighbor nodes that are outside the band region. The weights of the edges connecting the boundary nodes with the multiple sources and sinks are computed similarly to the n-links and then are cumulated to obtain the weights of the t-links in the corresponding single-source and single-sink graph. Thus, the computation is complicated. Moreover, because the weights of the t-links are not ensured to be infinite, we cannot avoid

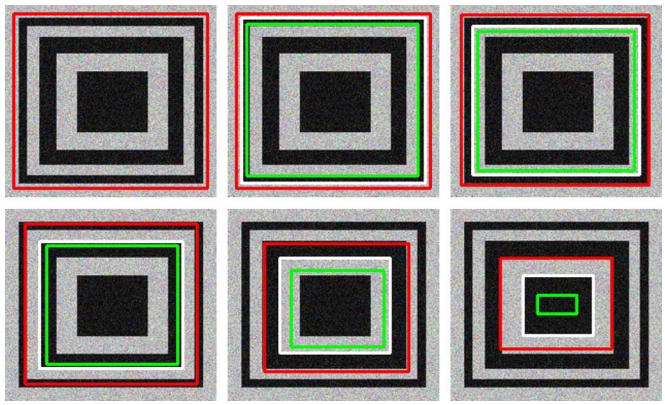

Fig. 5. INBBGC algorithm is tested. (From left to right) Row 1: (Red) The initial curve, the result with parameter $d = 10$, and the result with parameter $d = 20$. (From left to right) Row 2: The result with parameter $d = 27$, the result with parameter $d = 35$, and the result with parameter $d = 45$. The image size is 400×350. In each result image, the white curve is the result curve after convergence, and the red and green curves are the exterior and interior boundaries of the band graph, respectively.

partition the nodes of the interior boundary and the exterior boundary into the same part, which will lead to some meaningless results. Although this case does not appear in most applications because the weight of every t-links is cumulatively computed and is much larger than the weight of the n-links, the latent instability still is not eliminated.

IV. IINBBGC for Minimization of GACWRFs

We have previously said that due to the intrinsic limitation of the energy functional derived from the GAC, the global minimization of the GAC model corresponds to a point that has no practical sense. We devised an NBBGC method to solve the local minimizing problem of the GAC. In this band graph, only the nodes in the exterior and interior boundaries have t-links connecting the source and sink nodes. This NBBGC method can be extended to an iterative manner for less sensitivity to the initial curve. However, minimizing the energy function corresponding to the GAC model actually minimizes the integral of the image gradient along one curve. Therefore, besides preferring the curve with larger image gradient, the GAC model prefers the curve with a shorter length, which is just the reason why the GAC model has a bias of segmenting a smaller region. This favor to the shorter curve makes the GAC model hard to deal with the object that includes a concave region and complicated real-world images.

The examples in Fig. 6 analyze the defects of the INBBGC algorithm or the GCBAC algorithm [31]. The curve cannot evolve to the concaves when $d = 15$ (row 1 in Fig. 6). Increasing d to 30, this problem can be solved (row 2 in Fig. 6) due to a larger search range. However, this can lead to other problems. If we place a white rectangle curve inside the black object (row 3 in Fig. 6), the curve will converge to the white rectangle. This is because the white rectangle has smaller GAC energy than the boundary of the black object in the band region with $d = 30$.

If the region forces is integrated into the GAC and we use an IINBBGC method to optimize this model, this problem can be solved. In row 4 in Fig. 6, using the IINBBGC algorithm, the curve can evolve to the concave with just $d = 15$. In addition, in row 5 in Fig. 6, when the disturbed white rectangle is added, the IINBBGC algorithm can still converge to the right result with $d = 30$. We next describe the model of the GAC with region forces and the IINBBGC algorithm.

A. GACWRFs

The original GAC model can be called the boundary force since it is just related to the gradient and length of the evolving curve. To overcome this problem mentioned above, we introduce region force to the GAC model. The region force is based on the feature of the image regions outside the evolving curve and inside the evolving curve. Therefore, the GACWRF model includes both the boundary and region forces and can be written as follows:

$$E(C) = E_r(C) + \lambda E_b(C). \tag{19}$$

The region force can be divided into the exterior and interior region forces. Assume that we know the color distribution of the foreground and the background in prior, then the interior region force will prefer the nodes that are similar to the distribution of the foreground, and the exterior region force will prefer the nodes that are similar to the distribution of the background. Given the color distribution of the foreground and the background are respectively $C_f(x, y)$ and $C_b(x, y)$, the interior and exterior region forces can be defined as

$$E_{\mathrm{ri}}(C) = \iint\limits_{\Omega_1 \cap R_b} |C_f(x, y) - u_0(x, y)| \tag{20}$$

$$E_{\mathrm{re}}(C) = \iint\limits_{\Omega_2 \cap R_b} |C_b(x, y) - u_0(x, y)| \tag{21}$$

where Ω_1 is the region inside evolving curve C, Ω_2 is the region outside C, and R_b is the band region formed by dilating curve C.

Then, we have

$$\begin{aligned} E_r(C) = & \iint\limits_{\Omega_1 \cap R_b} |C_f(x, y) - u_0(x, y)| \\ & + \iint\limits_{\Omega_2 \cap R_b} |C_b(x, y) - u_0(x, y)| \end{aligned} \tag{22}$$

$$\begin{aligned} E(C) = & E_r(C) + \lambda E_b(C) \\ = & \iint\limits_{\Omega_1 \cap R_b} |C_f(x, y) - u_0(x, y)| \\ & + \iint\limits_{\Omega_2 \cap R_b} |C_b(x, y) - u_0(x, y)| \\ & + \lambda \int_0^{L(C)} g\left(C(s)\right) ds. \end{aligned} \tag{23}$$

It should be noticed that energy function (23) is defined in band region R_b, not in the whole image domain $\Omega = \Omega_1 + \Omega_2$.

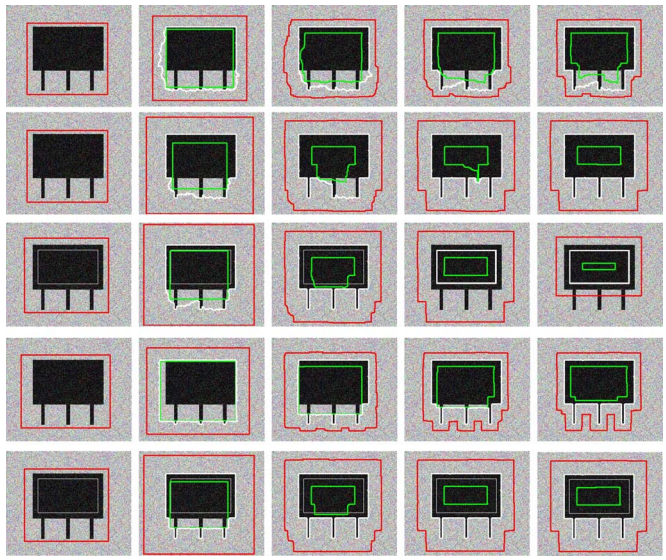

Fig. 6. INBBGC and GCBAC algorithms [31] are used on rows 1, 2, and 3, and the IINBBGC algorithm with SMM is used on rows 4 and 5. From columns 1 to 5: The image and the initial curve, the result of the first iteration, the result of the second iteration, the result of the third iteration, and the result of the fourth iteration. The images used in rows 1, 2, and 4 are the same, and the images used in rows 3 and 5 are the same and are added a white rectangle in the image used in rows 1, 2, and 4. Parameter $d = 15$ for rows 1 and 4. $d = 30$ for rows 2, 3, and 5. The image size is 240 × 280. (Thick white curve) The result curve after every iteration. The red and green curves are, respectively, the exterior and interior boundaries of the band graph in every iteration. The algorithm in rows 1–4 converges after four iterations; the algorithm in row 5 converges after three iterations.

B. IINBBGC for Minimization of the GACWRF

We will show that the region force defined in (22) can be transformed to the t-links of band graph $\mathbf{G}$ that we construct in Section III. Then, the energy function defined in (23) can be minimized by the graph cuts framework.

Considering binary variable x_{ij} defined in (9) and let $p = (i,j) \in \Omega$, the discrete representation of (22) is as follows:

$$E_r'(C) = \sum_{p \in R_b} |C_f(p) - u_0(p)|\, x_p + \sum_{p \in R_b} |C_b(p) - u_0(p)|\, (1 - x_p). \quad (24)$$

Therefore, the discrete form of the whole energy function in (23) is as follows:

$$\begin{aligned} E'(C) &= E_r'(C) + \lambda E_b'(C) \\ &= \sum_{p \in R_b} |C_f(p) - u_0(p)|\, x_p \\ &\quad + \sum_{p \in R_b} |C_b(p) - u_0(p)|\, (1 - x_p) \\ &\quad + \lambda \sum_{p,q \in R_b} \sum_{p \in N(q)} \frac{\omega_{pq}}{1 + \beta\, |u_0(p) - u_0(q)|} \\ &\quad \times ((1 - x_p) x_q + x_p (1 - x_q)). \end{aligned} \quad (25)$$

Energy functional (25) is a typical energy function that can be optimized by graph cuts method [35]. Notice that in constructed graph $\mathbf{G}$ based on band region R_b in Section III, only the nodes in the interior and exterior boundaries of band graph $\mathbf{G}$ have t-links with infinite weights. We additionally add t-links to the middle nodes in the band graph, and the weights can be computed as follows:

$$w_{sp} = |C_b(p) - u_0(p)| \quad (26)$$

$$w_{pt} = |C_f(p) - u_0(p)|. \quad (27)$$

It should be noticed that, in this graph, the weights of the t-links of the nodes in the interior and exterior boundaries of the band graph are still infinite, which insure that the minimum cut curve includes the interior boundary of band region R_b. In a practical application, due to the introduction of the region forces, besides the close curve that includes the interior boundary of band region R_b, the result curves corresponding to the minimum cut include some other short curves that do not include the interior boundary of R_b. We can filter out those curves that do not include the interior boundary of R_b and just retain the one that include the interior boundary, which corresponds to the minimization of the GAC with region forces in band region R_b. If multiple interior contours form in band region R_b during the iterative process, the evolving curve will automatically split into multiple curves. Thus, multiple object boundaries will be extracted. We will testify this case in the next experiments.

We have previously assumed that the color distribution of the foreground $C_f(p)$ and the color distribution of the background $C_b(\mathrm{b})$ are known in prior. Then, we can use (26) and (27) to compute the t-links of the middle nodes in band graph $\mathbf{G}$. However, the prior distributions of the foreground and background are difficult to obtain in advance due to the complexity and multiplicity of the natural scene images. We solve this problem by learning the distributions of the foreground and background according to the information of the regions inside and outside evolving curve C and then iteratively solve the minimum cut problem of band graph $\mathbf{G}$ and update the distributions of the foreground and background until the algorithm converges. Therefore, we can obtain an IINBBGC method to solve the minimization of the GACWRF model as follows.

IINBBGC Algorithm:

1) Initialize curve C and learn the distributions of the foreground and background according to the information of the regions inside and outside C.

2) Dilate curve C to form band region R_b.

3) Consider the pixels of band region R_b as the nodes of $\mathbf{G}$, and construct flow network graph $\mathbf{G}$ corresponding to R_b. Every node has two t-link connecting the source and sink nodes. The weights of the t-links of the nodes in the interior and exterior boundaries of $\mathbf{G}$ are set infinite. The weights of the other t-links are computed by (26) and (27). The weights of the ns-links are computed according to (18).

4) Compute the minimum cut $(\mathbf{S}, \mathbf{T})$ with $s \in S = \{p : x_p = 1\}$ and $t \in T = \{p : x_p = 0\}$ of $\mathbf{G}$ using the graph cuts algorithm, get close curve $C_{\min}$ corresponding to the minimization of the GAC with the region forces, and filter out the other curves that do not include the interior boundary of $\mathbf{G}$.

5) Learn the distribution of foreground $C_f(p)$ according to the information of the region inside $C_{\min}$ and the distribution of background $C_b(p)$ according to the information of the region outside $C_{\min}$. Dilate curve $C_{\min}$ to update band region R_b.

6) Repeat from steps 3 to 5 until the algorithm converges.

7) Consider the pixels of the image region inside curve $C_{\min}$ as the foreground and the pixels of the image region outside curve $C_{\min}$ as the background. We can obtain the image segmentation results.

In all our experiments, this algorithm converged in 6–12 iterations. In the proposed model in (23), the boundary force requires the result curve to favor larger gradient and shorter length, and the region force requires the region inside the result curve to be more similar to the prior foreground distribution and the region outside the result curve to be more similar to the prior background distribution. We now introduce two region force models to compute the region forces. One is MM, and the other is PM.

MM: The MM includes the single MM (SMM) and multiple MM (MMM). The SMM simply models the regions inside

evolving curve C and outside C by their mean color of all the pixels in the regions, respectively. This is to say that $C_f(p)$ is the average c_f of the pixels inside C, and $C_b(p)$ is the average c_b of the pixels outside C. Then, (26) and (27) can be rewritten as follows:

$$w_{sp} = |c_b - u_0(p)| \tag{28}$$

$$w_{pt} = |c_f - u_0(p)|. \tag{29}$$

Using SMM region force, our proposed IINBBGC method is somewhat similar to the method by El-Zehiry *et al.* [39], where the CV model by Chan and Vese [36] has been optimized by the graph cuts method. One difference is that the third term of our energy function (23) is the GAC, which is the integral of the image gradient along one curve, and the third term of the energy function in [39] is the length of one curve. The other difference is that the minimization of our energy function is based on one band region, and the minimization of the energy function in [39] is based on the whole image. When the SMM region force is used and the narrowband is extended to the whole image, our energy function can be regarded as a mixed model that integrates the CV and GAC models, which has been studied in [11], [13], and [14].

When the SMM region force is used in the GACWRF model, the same disadvantage still exists as in the CV model that the intensity inhomogeneity of the object segmentation cannot be effectively handled. This problem can be overcome by MMM, modeling the regions inside C and outside C using multiple constant values, instead of only one constant. We first cluster the regions inside C and outside C into k subset by k-means method, respectively, then respectively compute the k means c_{fi} and c_{bi} $(i = 1, \ldots, k)$ of the k subsets of the regions inside C and outside C. In this case, (26) and (27) can be rewritten as follows:

$$w_{sp} = \min_{i=1}^{k} |c_{bi} - u_0(p)| \tag{30}$$

$$w_{pt} = \min_{i=1}^{k} |c_{fi} - u_0(p)|. \tag{31}$$

PM: The PM assumes that the regions inside C and outside C obey two probability distributions. Assume that the two probability density functions are respectively $h_f(u_0(p))$ and $h_b(u_0(p))$. Inspired by the well-known statistical energy function optimized by the graph cuts method in many literatures [15]–[17], [20], [21], the region forces can be defined as

$$w_{sp} = -\log(h_b(u_0(p)) \tag{32}$$

$$w_{pt} = -\log(h_f(u_0(p)). \tag{33}$$

We can select the common used Gaussian probability distribution to model $h_f(u_0(p))$ and $h_b(u_0(p))$. Moreover, Gaussian model (GM) can be easily extended to GMM for more robust performance just like [21] does. In this case, the IINBBGC method is similar to Grabcut [21] despite our method being based on variational formulations, i.e., the GACWRF model, and the Grabcut method is based on a statistical formulation [15], [19], [21], [37]. The one difference is that our proposed IINBBGC method is based on one band region of the image, and the Grabcut [21] is based on the whole image. Thus, the Grabcut method can be regarded as the special case of the proposed IINBBGC method when the band region is extended to the whole image, and the GMM region force is used. The other difference is the computation of the n-links. In our method, the n-links is computed according to (18), which is not only related to the image gradient but also the neighbor system, which is deduced by the cut metric theory on the graph [22]. The computation of n-links in the Grabcut method is just related to the image gradient.

V. Experimental Results

Here, we will testify our proposed IINBBGC method using synthetic and real images. We will show the iterative process of some example images and demonstrate how our algorithm can converge to the boundary of the objects. Our IINBBGC method cannot only effectively overcome the sensitivity to the initial curve and the local image gradient but also can automatically split from one contour to multiple contours during the evolution. This good feature makes our method extract multiple object boundaries in the image at the same time. We will also show that the IINBBGC algorithm is more powerful than the INBBGC algorithm, which is analyzed similar to the GCBAC algorithm in [31]. To design the region forces, we have presented two kinds of models: MM and PM. The MM includes SMM and MMM. For the PM, we adopt the GM and its extension, i.e., GMM. In our numerical experiment, the GMM can better model the region forces of the IINBBGC algorithm, compared with the other region force models. We present some compared experiment of the four region force models. We also compare the performance of our proposed IINBBGC algorithm with the Grabcut [21] and GCBAC methods [31] because the IINBBGC algorithm can be regarded as a narrow-band-based Grabcut method or GCBAC with the region force method. Since, for most test images, the INBBGC algorithm can obtain almost the same results as the GCBAC algorithm [31], in the following experiment, we just test the INBBGC algorithm and compare it with our proposed IINBBGC algorithm.

We first use two synthetic images in Figs. 6 and 7 to test and compare the IINBBGC algorithm with the INBBGC and GCBAC algorithms [31]. In Fig. 7, the synthetic image includes some thin and deep concave regions and is more complicated than the synthetic image in Fig. 6. From row 2 in Fig. 6, we can see that the curve can evolve to the concave using the INBBGC algorithm or the GCBAC algorithm with $d = 30$. However, in Fig. 7, see row 4, without region forces, the curve cannot evolve to the thin and deep concaves using the INBBGC algorithm with $d = 30$. When the region forces is integrated, see the iterative process shown in rows 1–3 in Fig. 7, the boundary of the object can be accurately extracted using the IINBBGC algorithm with $d = 10$.

Fig. 8 shows the extracting process of two detached objects using the INBBGC algorithm or the GCBAC algorithm. We can see that the initial curve can be split into two curves to extract two objects as the iterative progresses. However, for the test image in Fig. 9, from row 4 in Fig. 9, we can see that

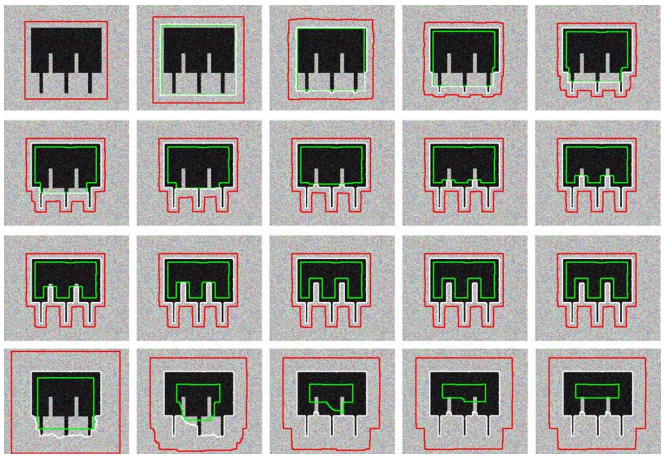

Fig. 7. Rows 1–3 are the iterative processes of the IINBBGC algorithm with the SMM and $d = 10$; the algorithm converges after 12 iterations. Row 4 is the iterative process of the INBBGC and GCBAC algorithms [31] with $d = 30$; the algorithm converges after five times. The top left is the image and the initial curve. The image size is 240×280. The red and green curves are, respectively, the exterior and interior boundaries of the band graph in every iteration. (White curve) The result curve after every iteration.

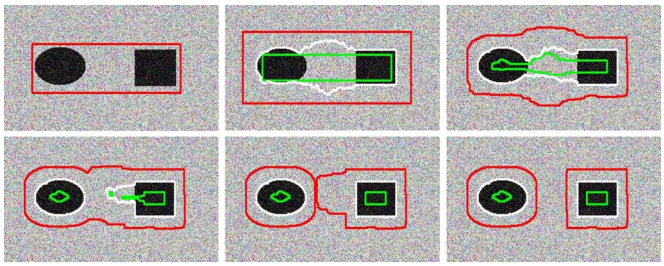

Fig. 8. INBBGC and GCBAC algorithms [31] are tested. The image includes two objects and the iterative process of the INBBGC algorithm with $d = 15$. The red and green curves are, respectively, the exterior and interior boundaries of the band graph in every iteration. (White curve) The result curve after every iteration.

however parameter d is changed (from 10 to 40), the objects cannot be accurately extracted by the INBBGC algorithm or the GCBAC algorithm because the distances between the objects are so narrow that the curve cannot evolve to the concaves without region forces. Rows 1–3 in Fig. 9 is the iterative process of the IINBBGC algorithm with $d = 10$. We can see that the curve is gradually split to extract multiple objects as the iteration progresses. The plots of the energy value of the iterative process for the images in Figs. 6, 7, and 9 are shown in column 1 in Fig. 18.

Even though synthetic images allow us to precisely demonstrate the goodness of the segmentation method and enable a direct comparison with related approaches, the use of real-world images is more interesting and can also provide insights into the segmentation performance. Moreover, real-world natural images are much more complicated than synthetic images, which makes many methods that are effective to synthetic images cannot be applied to real-world image processing applications. In the next experiments, we mainly test the performance of the proposed method by using real-world images.

The experiments in Figs. 10–12 demonstrate the iterative processes of three real-world images by our proposed IINBBGC algorithm with the GMM region force. All of these images can be effectively handled, and the objects are perfectly extracted. The plots of the energy value of the iterative process for the images in Figs. 10–12 are shown in column 2 in Fig. 18. The results of the three images used in Figs. 10–12 by the INBBGC and GCBAC algorithms are shown in Fig. 13. We can see that the GCBAC and INBBGC algorithms perform not well for the real-world images. In Fig. 14, we test the NBBGC algorithm by manually placing the interior and exterior boundaries. Although we carefully place the initial boundaries as close to the boundary of the real objects in images as possible, the results still are not ideal.

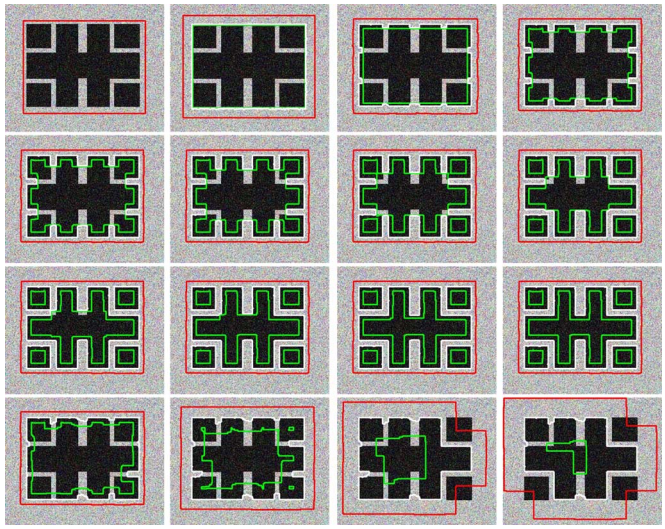

Fig. 9. Rows 1–3 is the iterative process by the IINBBGC algorithm with the SMM and $d = 10$, the algorithm converges after ten iterations. Row 4 is the test results of the INBBGC and GCBAC algorithms [31]. (From left to right) The result with $d = 10$ after convergence, the result with $d = 20$ after convergence, the result with $d = 30$ after convergence, and the result with $d = 40$ after convergence. The top left is the image and the initial curve; the image size is 240×280. The red and green curves are, respectively, the exterior and interior boundaries of the band graph in every iteration. (White curve) The result curve after every iteration.

Fig. 10. Iterative process of the image with two horses is shown. The IINBBGC algorithm with the GMM region force is used, parameter $k = 3$, and $d = 15$. The algorithm converges after seven iterations. The red and green curves are, respectively, the exterior and interior boundaries in every iteration. (White curve) The result curve after every iteration. The image size is 384×256.

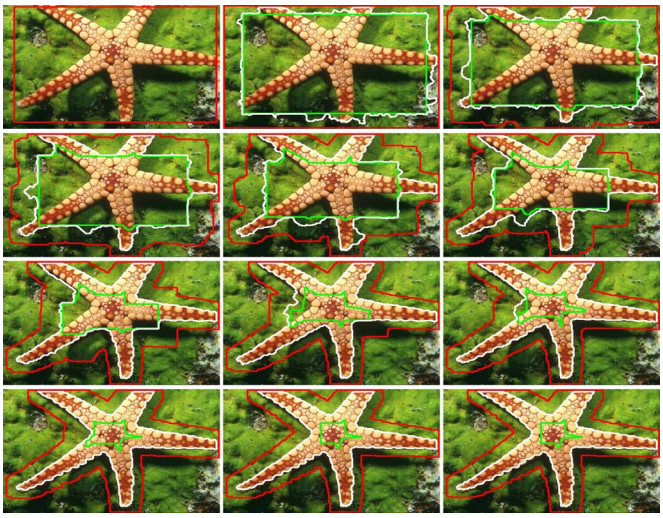

Fig. 11. Iterative process of the pentacle image is shown. The IINBBGC algorithm with the GMM region force is used, parameter $k = 3$, and $d = 15$. The algorithm converges after ten iterations. The red and green curves are, respectively, the exterior and interior boundaries in every iteration. (White curve) The result curve after every iteration. The image size is 384 × 256.

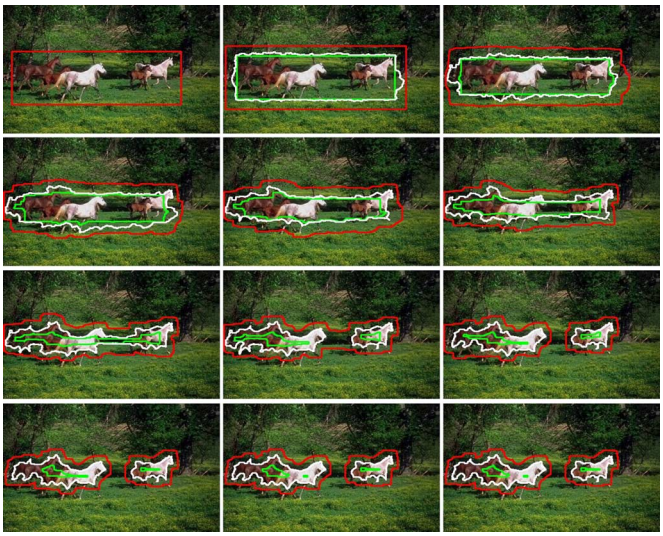

Fig. 12. Iterative process of the image with two group horses is shown. The IINBBGC algorithm with the GMM region force is used, parameter $k = 3$, and $d = 15$. The algorithm converges after ten iterations. The red and green curves are, respectively, the exterior and interior boundaries in every iteration. (White curve) The result curve after every iteration. The image size is 384 × 256.

Fig. 13. INBBGC and GCBAC algorithms are tested with parameter $d = 15$. (White curve) The result curve after convergence. The red and green curves are, respectively, the exterior and interior boundaries of the band graph. The initial curves of the three images are the same as in Figs. 10–12.

In Fig. 15, the IINBBGC algorithm with the other three region forces such as SMM, GM, and MMM is tested. From the compared results, we can see that although SMM can effectively

Fig. 14. NBBGC algorithm is tested, and the interior and exterior initial curves are carefully placed by the user. (White curve) The result curve. The red and green curves are, respectively, the placed exterior and interior boundaries by the user.

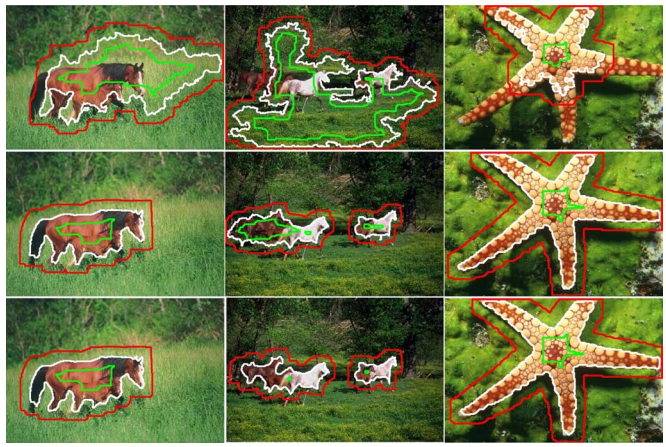

Fig. 15. IINBBGC algorithm is tested. Row 1 is the results using the SMM region force. Row 2 is the results using the GM region force. Row 3 is the results using the MMM region force with $k = 5$. Parameter $d = 15$. The red and green curves are, respectively, the exterior and interior boundaries. (White curve) The result curve. The initial curves of the three images are the same as in Figs. 10–12.

deal with the synthetic images in Figs. 6, 7, and 9, the ability to process real-world images is very bad. The reason is that the objects in the images in Figs. 10–12 have inhomogeneous intensity distribution, and using the IINBBGC algorithm with the SMM region force, the same disadvantage exists, as in the CV model that the intensity inhomogeneity of the object segmentation cannot be effectively handled. Comparatively, the results by MMM and GM region forces are both acceptable but a little worse than the GMM region force.

The experiment in Fig. 16 is a special case of the IINBBGC algorithm with the GMM region force, where the interior boundary disappears after two iterations due to a large value of 30 of parameter d. In this case, the INBBGC algorithm or GCBAC algorithm will converge to one point and lead to a meaningless segmentation. However, using the proposed IINBBGC algorithm with the GMM region force, the balance of the region forces ensures that the evolving curve can converge to a feasible local minimization.

The experiment in Fig. 17 is a more special case of the IINBBGC algorithm than in Fig. 16, where both the interior and exterior boundaries of the band region disappear during the iterative process. In this case, the IINBBGC algorithm with GMM region force model is equivalent to the Grabcut method [21]. We respectively test the four region forces using the three real images in the previous experiments. The result by [39] is also shown in row 2 in Fig. 17. The results by the SMM region force in row 3 in Fig. 17 are just the results of the graph cuts optimization of the CV-GAC model. From the

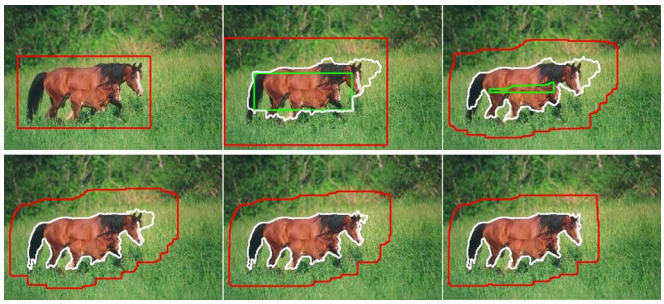

Fig. 16. IINBBGC algorithm with the GMM region force is tested, parameter $k = 3$, and $d = 30$. The interior boundary disappears after two iterations. The red and green curves are, respectively, the exterior and interior boundaries in every iteration. (White curve) The result curve after every iteration.

Fig. 17. IINBBGC algorithm with four region forces is tested, and the band region is extended to the whole image. In this case, the IINBBGC algorithm with the GMM region force is equivalent to the Grabcut method [21]. The comparison with [39] is also conducted. From rows 1 to 6: The original image and the initial curve, the result by [39], the result by the SMM region force, the result by the MMM region force with $k = 5$, the result by the GM region force, and the result by the GMM region force with $k = 3$. (White curves) The result contours.

results, we can see that all the results are worse than that in Figs. 10–12 due to the too large search space in each iteration (see Fig. 18).

VI. Conclusion

In this paper, we have first deduced the discrete representation of the GACs based on cut metric on graphs and then devised an NBBGC method to solve the local minimization of the GAC for higher efficiency and better accuracy than the traditional level set framework. An extension to an iterative manner, namely, INBBGC, is developed for less sensitivity to the initial curve. The sameness and difference between the INBBGC and GCBAC methods presented by Xu *et al.* [31] have been analyzed and discussed. We then integrate the region force into the GAC. An IINBBGC method has been proposed to optimize the GACWRF model and can thus effectively deal with the concave region and complicated real-world image segmentation. Two region force models such as the MM and the PM are studied. Our proposed IINBBGC method can be analytically regarded as a narrow-band-based Grabcut method or the GCBAC with the region force method. A large number of synthetic and real-world images are tested to emphasize the performance of our model, compared with other segmentation methods.

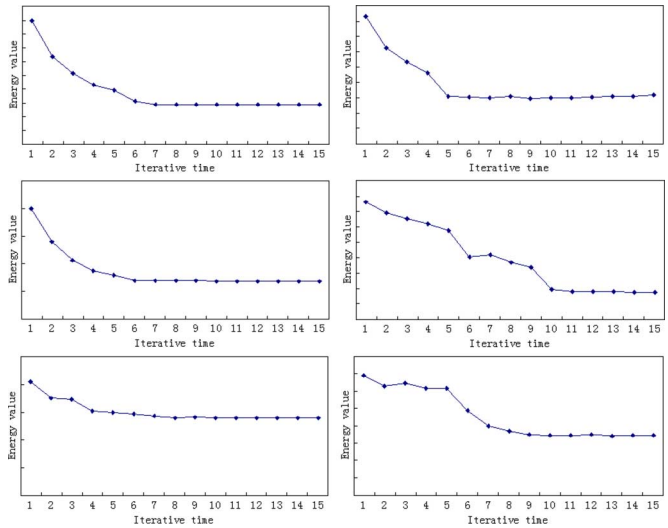

Fig. 18. Plot of the energy value for the iterative process of the IINBBGC algorithm. The iterative time is 15. The horizontal and the vertical axes denote the iterative times and the energy value, respectively. (From top to bottom) Column 1: The synthetic image in Fig. 6, the synthetic image in Fig. 7, and the synthetic image in Fig. 9. (From top to bottom) Column 2: The real image in Fig. 10, the real image in Fig. 11, and the real image in Fig. 12.

References

[1] M. Kass, A. Witkin, and D. Terzopoulos, "Snakes: Active contour models," *Int. J. Comput. Vis.*, vol. 1, no. 4, pp. 321–331, 1987.
[2] V. Caselles, R. Kimmel, and G. Sapiro, "Geodesic active contours," *Int. J. Comput. Vis.*, vol. 22, no. 1, pp. 61–79, Feb./Mar. 1997.
[3] R. Goldenberg, R. Kimmel, E. Rivlin, and M. Rudzsky, "Fast geodesic active contours," *IEEE Trans. Image Process.*, vol. 10, no. 10, pp. 1467–1475, Oct. 2001.
[4] C. Xu and J. L. Prince, "Snakes, shapes, and gradient vector flow," *IEEE Trans. Image Process.*, vol. 7, no. 3, pp. 359–369, Mar. 1998.
[5] N. Sochen, R. Kimmel, and R. Malladi, "A general framework for low level vision," *IEEE Trans. Image Process.*, vol. 7, no. 3, pp. 310–318, Mar. 1998.
[6] L. D. Cohen and I. Cohen, "Finite-element methods for active contour models and balloons for 2-D and 3-D images," *IEEE Trans. Pattern Anal. Mach. Intell.*, vol. 15, no. 11, pp. 1131–1147, Nov. 1993.
[7] L. D. Cohen and R. Kimmel, "Global minimum for active contour models: A minimal path approach," *Int. J. Comput. Vis.*, vol. 24, no. 1, pp. 57–78, 1997.
[8] J. Sethian, "A fast marching level set method for monotonically advancing fronts," *Proc. Nat. Acad. Sci. U. S. A.*, vol. 93, no. 4, pp. 1591–1595, Feb. 1996.
[9] L. D. Cohen, "Multiple contour finding and perceptual grouping using minimal paths," *J. Math. Imag. Vis.*, vol. 14, no. 3, pp. 225–236, May 2001.

[10] B. Appleton and H. Talbot, "Globally optimal geodesic active contours," *J. Math. Imaging Vis.*, vol. 23, no. 1, pp. 67–86, Jul. 2005.
[11] X. Bresson, S. Esedoglu, P. Vandergheynst, J.-P. Thiram, and S. Osher, "Fast global minimization of the active contour/snake model," *J. Math. Imaging Vis.*, vol. 28, no. 2, pp. 151–167, Jun. 2007.
[12] L. I. Rudin, S. Osher, and E. Fatemi, "Nonlinear total variation based noise removal algorithms," *Phys. D*, vol. 60, no. 1–4, pp. 259–268, Nov. 1992.
[13] D. Mumford and J. Shah, "Optimal approximations by piecewise smooth functions and associated variational problems," *Commun. Pure Appl. Math.*, vol. 42, no. 5, pp. 577–685, Jul. 1989.
[14] D. Mumford and J. Shah, "Boundary detection by minimizing functionals," in *Proc. IEEE Comput. Soc. Conf. Comput. Vis. Pattern Recognit.*, 1985, pp. 22–26.
[15] D. Greig, M. B. T. Porteous, and A. H. Seheult, "Exact maximum a posteriori estimation for binary images," *J. Roy. Stat. Soc. B*, vol. 51, no. 2, pp. 271–279, 1989.
[16] Y. Boykov, O. Veksle, and R. Zabih, "Fast approximate energy minimization via graph cuts," *IEEE Trans. Pattern Anal. Mach. Intell.*, vol. 23, no. 11, pp. 1222–1239, Nov. 2001.
[17] Y. Boykov and V. Kolmogorov, "An experimental comparison of min-cut/max-flow algorithms for energy minimization in vision," *IEEE Trans. Pattern Anal. Mach. Intell.*, vol. 26, no. 9, pp. 1124–1137, Sep. 2004.
[18] Y. Boykov, V. Kolmogorov, D. Cremersm, and A. Delong, "An integral solution to surface evolution PDEs via Geo-Cuts," in *Proc. ECCV*, 2006, pp. 409–422.
[19] Y. Boykov and G. Funka-Lea, "Graph cuts and efficient N-D image segmentation," *Int. J. Comput. Vis.*, vol. 70, no. 2, pp. 109–131, Nov. 2006.
[20] Y. Li, J. Sun, C. K. Tang, and H. Y. Shum, "Lazy snapping," in *Proc. SIGGRAPH Conf.*, 2004, pp. 303–308.
[21] C. Rother, V. Kolmogorov, and A. Blake, "GrabCut: Interactive foreground extraction using iterated graph cuts," *ACM Trans. Graph.*, vol. 23, pp. 309–314, 2004.
[22] Y. Boykov and V. Kolmogorov, "Computing geodesics and minimal surfaces via graph cuts," in *Proc. ICCV*, 2003, pp. 26–33.
[23] A. Chambolle, "Total variation minimization and a class of binary mrf models," in *Energy Minimization Methods in Computer Vision and Pattern Recognition*. Berlin, Germany: Springer-Verlag, 2005, pp. 136–152.
[24] J. Darbon and M. Sigelle, "Image restoration with discrete constrained total variation Part I: Fast and exact optimization," *J. Math. Imaging Vis.*, vol. 26, no. 3, pp. 261–276, Dec. 2006.
[25] D. Kirsanov and S. Gortler, A discrete global minimization algorithm for continuous variational problems Harvard CS, Cambridge, MA, Tech. Rep. TR-14-04, 2004.
[26] D. Fulkerson and L. Ford, *Flows in Networks*. Princeton, NJ: Princeton Univ. Press, 1962.
[27] E. A. Dinic, "Algorithm for solution of a problem of maximum flow in networks with power estimation," *Soviet Math. Dokl.*, vol. 11, pp. 1277–1280, 1970.
[28] A. V. Goldberg and R. E. Tarjan, "A new approach to the maximum flow problem," in *Proc. 18th Annu. ACM Symp. Theory Comput.*, 1986, pp. 136–146.
[29] Z. Y. Wu and R. Leahy, "An optimal graph theoretic approach to data clustering: Theory and its application to image segmentation," *IEEE Trans. Pattern Anal. Mach. Intell.*, vol. 15, no. 11, pp. 1101–1113, Nov. 1993.
[30] J. Shi and J. Malik, "Normalized cuts and image segmentation," *IEEE Trans. Pattern Anal. Mach. Intell.*, vol. 22, no. 8, pp. 888–905, Aug. 2000.
[31] N. Xu, N. Ahuja, and R. Bansal, "Object segmentation using graph cuts based active contours," in *Proc. CVPR*, 2003, pp. II-46–II-53.
[32] S. Osher and R. Fedkiw, *Level Set Methods and Dynamic Implicit Surfaces*. New York: Cambridge Univ. Press, 2003.
[33] S. Osher and R. Tsai, "Level set methods and their applications in image science," *Commun. Math. Sci.*, vol. 1, no. 4, pp. 1–20, 2003.
[34] S. Han, W. Tao, D. Wang, X.-C. Tai, and X. Wu, "Image segmentation based on GrabCut frame integrating multi-scale nonlinear structure tensor," *IEEE Trans. Image Process.*, vol. 18, no. 10, pp. 2289–2302, Oct. 2009.
[35] V. Kolmogorov and R. Zabih, "What energy functions can be minimized via graph cuts?," *IEEE Trans. Pattern Anal. Mach. Intell.*, vol. 26, no. 2, pp. 147–159, Feb. 2004.
[36] T. Chan and L. Vese, "Active contours without edges," *IEEE Trans. Image Process.*, vol. 10, no. 2, pp. 266–277, Feb. 2001.
[37] S. Geman and D. Geman, "Stochastic relaxation, Gibbs distributions, and the Bayesian restoration of images," *IEEE Trans. Pattern Anal. Mach. Intell.*, vol. PAMI-6, no. 6, pp. 721–741, Nov. 1984.
[38] V. Kolmogorov and Y. Boykov, "What metrics can be approximated by geo-cuts, or global optimization of length/area and flux," in *Proc. ICCV*, 2005, pp. 564–571.
[39] N. El-Zehiry, P. Sahoo, S. Xu, and A. Almaghraby, "Graph cut optimization for the Mumford Shah model," in *Proc. 7th IASTED Int. Conf. VIIP*, 2007, pp. 182–187.
[40] S. Kichenassamy, A. Kumar, P. Olver, A. Tannenbaum, and A. Yezzi, "Gradient flows and geometric active contour models," in *Proc. ICCV*, 1995, pp. 810–815.

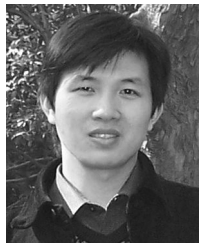

Wenbing Tao received the Ph.D. degree in pattern recognition and intelligent system from Huazhong University of Science and Technology (HUST), Wuhan, China, in 2004.

Since 2005, he has been with the School of Computer Science and Technology, HUST, where he was an Associate Professor. Now he is an Associate Professor of the Institute for Pattern Recognition and Artificial Intelligence, HUST. He was a Research Fellow in the Division of Mathematical Sciences, Nanyang Technological University, Singapore, from March 2008 to March 2009. His research interests are in the areas of computer vision, image segmentation, object recognition and tracking, image search engine, and multimedia retrieval. He has published numerous papers and conference papers in the area of image processing and object recognition.

Dr. Tao serves as a Reviewer for many journals, such as *International Journal of Computer Vision*, IEEE TRANSACTIONS ON IMAGE PROCESSING, *Pattern Recognition*, and *Image Vision Computing*.